Carbon Dioxide Methanation: design of a fully integrated plant

Antonio Tripodi, Francesco Conte, Ilenia Rossetti*

Chemical Plants and Industrial Chemistry Group, Dipartimento di Chimica, Università degli Studi di Milano, INSTM Milano Università-Unit, CNR-ISTM, Via Golgi 19, 20133 Milano (MI) – Italy

Abstract

A new, fully integrated process has been designed to evaluate the feasibility of the CO_2 methanation reaction according to the Sabatier reaction. This approach has two environmental advantages: i) the conversion of CO_2 into a regenerated fuel or platform chemical; ii) the chemical storage of H_2 to allow its long range transport using a well established distribution network.

Two kinetic models for the Sabatier reaction, reviewed from literature, were used to design a multistage plug-flow reactor. The outflowing gas was then purified from unreacted CO_2 and water and proper recycles were foreseen to achieve an overall 100% conversion of the CO_2, given that without water or methane withdrawal, at least 4 reactive stages are needed to get > 75% conversion. Either adiabatic or cooled catalytic beds can be used, operating at atmosphetic pressure below 400°C. This methanation process was set to the size of 10^5 Nm^3/day of synthetic methane. Process simulation under steady state conditions was used to calculate the stream compositions and the inner reactor thermal profile (9.2 MW, as determined by the reaction heat). The dehydration of the produced methane was accomplished by pressure-swing adsorption over a commercial basic zeolite and dynamically simulated. All the foreseen vapor-liquid equilibria have been carefully revised from literature data, in order to establish the separation sections on a firm basis. Two further calculations were given for the main energy recovery options and a possible downstream liquefaction.

Keywords: Carbon dioxide (CO_2); Methanation; Sabatier reaction; Process simulation; Dynamic pressure swing adsorption.

* Corresponding author: fax +39-02-50314300; email ilenia.rossetti@unimi.it

1. Introduction

As methane has been establishing itself as the primary energy source with respect to coal, though not without reserves [1], to obtain it from renewable carbon feedstock rather than to extract it as natural gas is even more appealing: biomass-generated methane would be the first option to have an efficient power generation with a virtually closed CO_2 cycle [2]. Furthermore, when renewable hydrogen is available its catalytic conversion into methane [3] would turn it into a species easier to handle, with an already existing distribution network (safe storage and transportation are still the main bottlenecks for hydrogen utilization far from its production sites). Different production methods for renewable hydrogen have been recently reviewed [4,5] and may be exploitable commercially in short time. However, they share the still unsolved problem of H_2 storage and distribution.

CO_2 hydrogenation to methane can be promising, as it implies the reuse of carbon dioxide captured in different contexts [2,6,7] (its sequestration strategies are more dependent on the specific geographic and technological environment [8]), and the transformation of an energy vector uneasy to handle (H_2) into a valuable and worldwide distributed fuel and feedstock. A "power-to-gas" framework could then help to overcome the drawbacks of hydrogen as an energy storage medium and to increase the continuity and general availability of different intermittent renewable energy sources [9–12]. This flexibility offers also additional possibilities for the downstream use of biogas, that may be richer in hydrogen or methane according to the process operation [13], even if these conditions might not fit the distribution networks nearer to the biomass treating site.

The efficient direct conversion of CO_2 and H_2 into CH_4 (Sabatier reaction) relies on the actual selectivity of the catalysts (based mainly on Ru or Ni), that is to say on their capability to shift the $CO \rightarrow CH_4$ conversion to completion after the CO_2 is partially reduced to CO. Ongoing research has been producing material that work in the medium temperature range 250 – 450 °C and different pressures [14–20]. Coking issues may be a problem, where most of the coking likely originates from CO reduction to carbon rather than to methane [21].

This work presents the overall design of a Sabatier process. Different power to gas technologies are reviewed elsewhere [10]. Catalytic methanation reactors are typically operated at temperatures between 200 °C and 550 °C and at pressures ranging from 1 to 100 bar. The catalysts are typically based on Ni, Ru, Rh and Co as active phase, Ni being the most used due to activity, selectivity and low cost. Different reactor concepts are compared. The simplest and most economic reactors arrangement is constituted of a certain number of adiabatic beds (up to 5) with intercooling. Some options proposed cooled stages, but are more expensive. Alternatives may be

fluidised bed reactors, that allow better temperature control, but lead to incomplete conversion and are more difficult to scale up. Furthermore, structured catalysts were proposed, using metallic supports to improve heat exchange, but catalyst replacement is critical. Overall, fixed bed reactors typically allow faster reaction.

Here we designed ex novo a CO_2 methanation plant, by linking the reaction kinetics to the gross plant balances up to the scale of 10^5 Nm^3 per day (corresponding roughly to the civil consumption only of a 70,000 people Italian town [22]). We identify the criticalities emerging from the available catalytic tests and propose a possible process layout for their solution. We also evaluate the options for the downstream treatment of the synthetic gas. With respect to other available process simulation [10] (and references therein), also the reactive stage is treated in detail following the guidelines reported elsewhere [23]. Overall, a fully integrated process has been here designed to evaluate the feasibility of the CO_2 methanation reaction. This approach has two environmental advantages: i) the conversion of CO_2 into a regenerated fuel or platform chemical; ii) the chemical storage of H_2 to favour its transport for long distances using a well established distribution/transport network. This is important especially for renewable H_2 produced far from the usage location. A well designed plant should be developed to ensure the feasibility and economic sustainability of the process.

2. Methods

2.1 Reaction Kinetics

The reaction of interest can be divided into two steps [15,16,21]:

$$CO_2 + H_2 \rightleftarrows CO + H_2O \qquad \Delta_r^0H = 41 \text{ kJ/mol} \qquad (1)$$

$$CO + 3H_2 \rightleftarrows CH_4 + H_2O \qquad \Delta_r^0H = -206 \text{ kJ/mol} \qquad (2)$$

We have carefully revised the available literature data and we have chosen kinetics candidates relative to very selective catalysts with negligible CO yield, so that the experimental tests could be treated with the lumped stoichiometry:

$$CO_2 + 4H_2 \rightleftarrows CH_4 + 2H_2O \qquad \Delta_r^0H = -165 \text{ kJ/mol} \qquad (3)$$

Between the various quantitative models available for reaction (3) [21], two have been selected and compared since they were complete, consistent, in the appropriate temperature and pressures range of interest. One is adequate for small conversions (χ) and low temperature (T) [15] (equation (4)), while another for the high conversion and high temperature rise [16] (equation (5)), since it details well the reverse reaction. In this case,

the test reactor was configured with the catalyst as a wall-coating film, then the material density and overall void fraction have been retrofitted in order to match the reported contact time to that of a packed-bed reactor, used for the present process calculation.

$$r_{\chi<0.1} = 3550 \left[\frac{mol/s}{kg \times kPa^{0.88}}\right] e^{-7950\ K/T} \left(\frac{P_{CO_2}^{0.34} P_{H_2}^{0.88}}{P_{CH_4}^{0.11} P_{H_2O}^{0.23}}\right) \quad (4)$$

$$r_{\chi>0.1} = 11.2 \left[\frac{mol/s}{kg\ \times bar^{1.5}}\right] e^{-2490\ K/T} \left(P_{CO_2}^{0.3} P_{H_2}^{1.2} - \frac{1}{K} P_{CH_4}^{0.3} P_{H_2O}^{0.6}\right) \quad (5)$$

Notice that the first formulation does not take explicitly into account the reactions reversibility (the products *slow down* the reaction rather than bringing on its reverse) and does not have exponents for the reactants partial pressures in the same ratio of their stoichiometric coefficients: this is due to the fact that the adopted conditions were sensitive to the adsorption kinetics of CO_2 onto the catalyst, but the obtained data have then been fitted to a simpler heuristic model.

The second equation, on the other hand, resorts to a heuristic constant multiplication factor for all the exponents, plus the activation energy, as: $r = \left(e^{E/RT}\right)^n \left[(\Pi\, P^{\upsilon})^n - \left(1/K\right)^n (\Pi\, P^{\upsilon})^n\right]$, where $ln\left(\frac{K}{bar^{-0.6}}\right) = 10.47 + \frac{5218}{T} - 2.55\ ln\, T + 0.00084\, T$.

Moreover, the data regression takes into account the transport phenomena foreseen in the particular reactor employed, so the derived intrinsic kinetic has not been obtained via tests where the reaction itself was the only relevant term in the mass balances. This aspect has been considered calculating contact times as close as possible to those tested in the reviewed paper. All the above mentioned data and formulas are relative to a total pressure of 1 atm. More complex models (see [24], [25] and references therein) are not strictly needed to give a basic representation of the products spectrum, especially when CO is not present in the feed.

Finally the steady-state mass and energy balances for the mono-dimensional reacting system were expressed as follows along the *z* coordinate:

$$0 = -\mathrm{u}' \frac{\partial n_i}{\partial z} + r\nu_i \left[\frac{mol/s}{kg}\right] \quad (6)$$

$$0 = -\mathrm{u}'' \frac{\partial h}{\partial z} + r\Delta h \left[\frac{J/s}{kg}\right] - U(T_r - T_c) \quad (7)$$

where n are the moles of the i-th species, r is the raction rate based on the catalyst load, ν_i the stoichiometric coefficients and u' is the local molar flow expressed as a function of the molar flowrate at the reactor inlet $\dot{n}$ and the actual concentration at the reactor conditions C(P,T), hydraulic section A and catalysts load w:

$u' = \frac{\dot{n}}{C(P,T)wA}\left[\frac{mol/s}{mol/_{m^3}\times kg\times m^2}\right]$; accordingly h represents the molar specific enthalpy and u'' is calculated in the same way. T_r, T_c are the reactants and coolant temperatures and U the overall heat transfer coefficient. The momentum balance is evaluated by a built-in Aspen Plus correlation and it affects indirectly the reaction rate and the spatial terms u', u''.

2.2 Process Layout

Already at this stage, three important process choice were made:

a) in order to control the released heat, the reactor was divided into several stages with step-wise cooling of the reacting mixture (each stage can be either adiabatic or cooled) – this is all the more important also because a low temperature enhances the methane yield at equilibrium, as proven by experimental tests [26];

b) the temperature rising is furtherly damped assuming to keep the conversion below 100% and adding steam to increase the overall thermal inertia, following the approach reported by Schaaf et al. [27], but with a different stream routing;

c) the recycle needed by the above provision is based on a CO_2 capture section based on a consolidated potassium carbonate scrubbing [28,29]: in this way the drawback of a recirculated reactor (larger volumes and catalyst loads) are minimized because the reactor products are not backrouted.

These essential criteria lead to a block scheme as the one reported in Figure 1. The CO_2 recycle and steam injection into the reactor are handled via the same macro-unit: in fact, the same LP steam used to regenerate the potassium-based scrubbing agent carries the stripped CO_2 to be mixed with the fresh feed. The steam is in turn generated using part of the water produced by the reaction. Within the scope of this work, only pure CO_2 and H_2 were considered as feed, to achieve general results: if the process is used to treat combustion gases, then the already present nitrogen helps to control the reactor temperature instead of additional steam [30,31]. In case a significant presence of CO should be reported for some feeds, well standardised methods for CO

conversion to CO_2 can be added to the process scheme. We have not considered this option here because it whould made the plant design too case sensitive.

A complete conversion of the CO_2 without recycling is possible also eliminating water before completing the reaction [32], but the solution presented here lets foresee a higher dew point for the condensing mixture, likely with better heat-recovery options. The choice of hot potassium carbonate as CO_2 entrainer [28,33,34] was made because the salt has a null equilibrium vapor pressure in the recycle stream at any temperature, avoiding its accumulation in the recycle loop and the need of purging and consequent make up.

Since the methane emerging from the potassium carbonate scrubbing still contains water vapor, it is dehydrated via the Pressure-Swing Adsorption (PSA) technique and the moisture recycled to the upstream CO_2 wash.

Though the reaction equilibrium is favored increasing the pressure, it is possible to achieve good single-pass conversions also at atmospheric pressure, which is also representative of the kinetic data used. The product compression, useful in the basic scrubbing and pressure-swing sections, is delayed after a first gross water condensation to save power.

Figure 1: Block scheme of the proposed Sabatier process with recycled reactor.

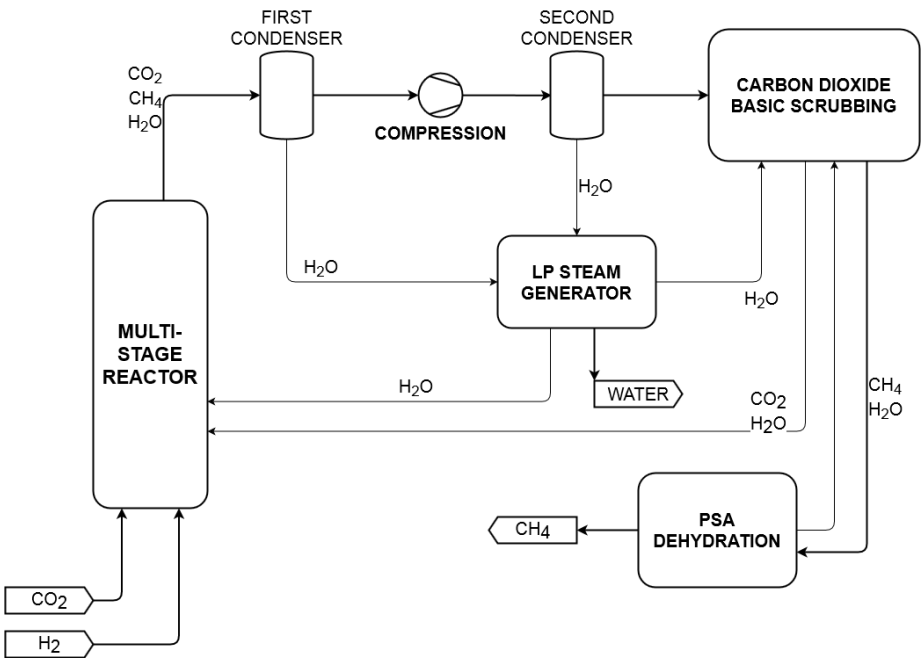

2.3 Software and models

The reactor calculation and the mass and energy balance of the other process blocks has been carried out using Aspen Plus® and Aspen Adsorption® by Aspen Technology Inc. (Bedford, MA, US). All the chemicals and the thermodynamic models employed are listed in **Table *1***. The ENRTL model has been used instead of the NRTL one to compute the activity coefficients in the presence of electrolytes. In combination with them, when computing the vapour liquid equilibria the Redlich-Kwong equation of state (EOS) has been selected. The solubility of gases in the liquid phase has been modelled through the Henry equation.

The next step has been the thorough review of the reliability of the different thermodynamic packages in describing the expected vapor-liquid equilibria (VLE), as summarized in Figure 2 to Figure ***7*** (data from [35–40]). The solubility in water of the gaseous components present in the various streams has been revised by analysis of the retrieved data at different pressure. The best fitting model (Henry equation) to be implemented in Aspen Plus® is reported in the same Figures, evidencing a good to acceptable agreement in the operating range selected. When needed, data were considered also in the presence of electrolytes, modifying the ionic strength of the solution, e.g. in the case of the CO_2-K_2CO_3-H_2O system. In particular, the solubility of hydrogen in water was underestimated above 40 °C, nevertheless a part of it was recovered as the process condensate is recycled into the reactor, so at fixed CO_2 conversion the global hydrogen balance is not affected and the impact on the steam generating section showed negligible.

Table 1: species and models involved in the calculation; potassium carbonate is present two times, because one identifier (POTAS-01) represents the substance regardless of its crystalline or solvated form and is used only as input for the mass balances.

Specie	Formula	MW (g/mol)	Report ID
Carbon Dioxide	CO_2	44	CARBO-01
Hydrogen	H_2	2	HYDRO-01
Methane	CH_4	16	METHA-01
Water	H_2O	18	WATER
Potassium Carbonate	K_2CO_3	138	POTAS-01
Hydronium	H_3O^+	19	$H3O^+$
Hydroxide	OH^-	17	OH^-
Potassium Cation	K^+	39	K^+

Potassium Carbonate	K_2CO_3	138	$K_2CO_{3(s)}$
Potassium Bicarbonate	$KHCO_3$	100	$KHCO_{3(s)}$
Bicarbonate	HCO_3^-	61	HCO_3^-
Carbonate	CO_3^{2-}	60	CO_3^{2-}

Model	**Type**	**Database**
PSRK	Equation of State (EoS)	APV90 EOS-LIT
NRTL-RK	Activity coefficient plus EoS	APV90 NRTL-RK
ENRTL-RK	Activity coefficient plus EoS	APV90 ENRTL-RK
HENRY	Henry constant	APV90 BINARY
REFPROP	Equation of State	NIST-REFPROP

The dissociation of potassium carbonate in water has been considered complete, as its concentration has always been kept below the saturation threshold, and even below other commonly adopted process conditions [41], while the aqueous equilibria between the charged carbonate species are described as follows:

$$CO_3^{2-} + H_3O^+ \rightleftarrows HCO_3^- + H_2O \qquad \ln K_6 = -216.05+12432/T+35.482 \ln T \qquad (8)$$

$$HCO_3^- + H_3O^+ \rightleftarrows CO_2 + H_2O \qquad \ln K_7 = -231.46+12092/T+36.782 \ln T \qquad (9)$$

$$2H_2O \rightleftarrows OH^- + H_3O^+ \qquad \ln K_8 = -132.90-13446/T-22.477 \ln T \qquad (10)$$

The Henry constants for CO_2 and CH_4 in presence of the electrolytes have been furtherly reviewed [42,43] and corrected when necessary (Figures 8-10). The latter Figures report how the gas solubility changes in the presence of a dissolved salt, which in turn modifies the ionic strength and the activity coefficients. Finally, to consider the presence of residual hydrogen into the methane stream, also this VLE [44] has been checked (Figure 11).

Figure 2: Solubility of methane in water at atmospheric pressure.

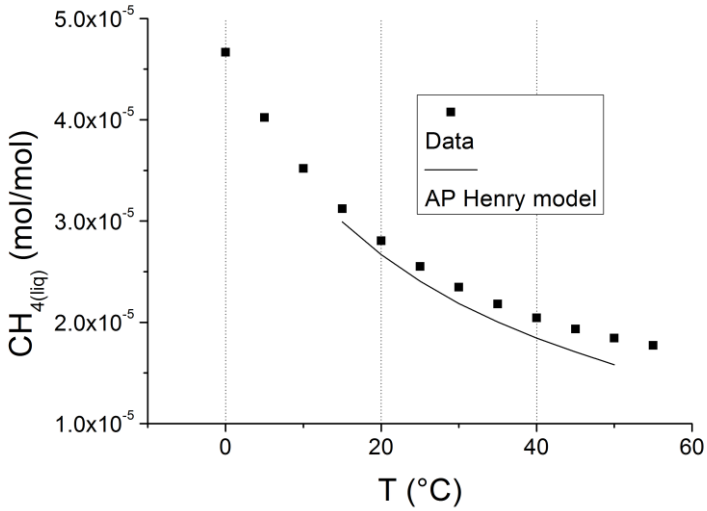

Figure 3: Solubility of methane in water at increasing pressure.

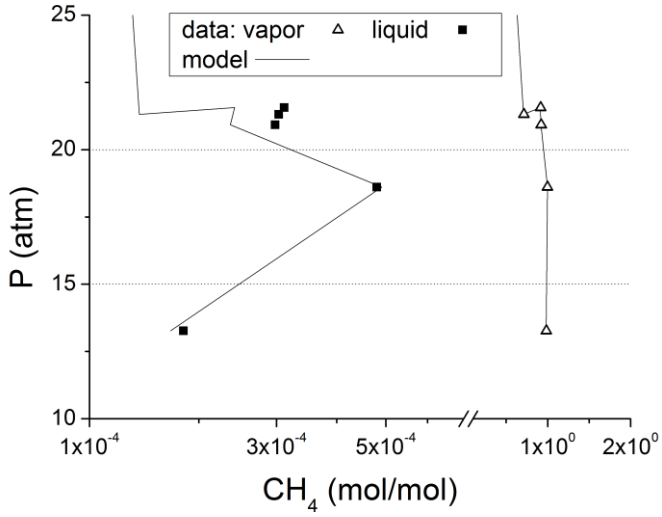

Figure 4: Solubility of CO_2 in water at atmospheric pressure.

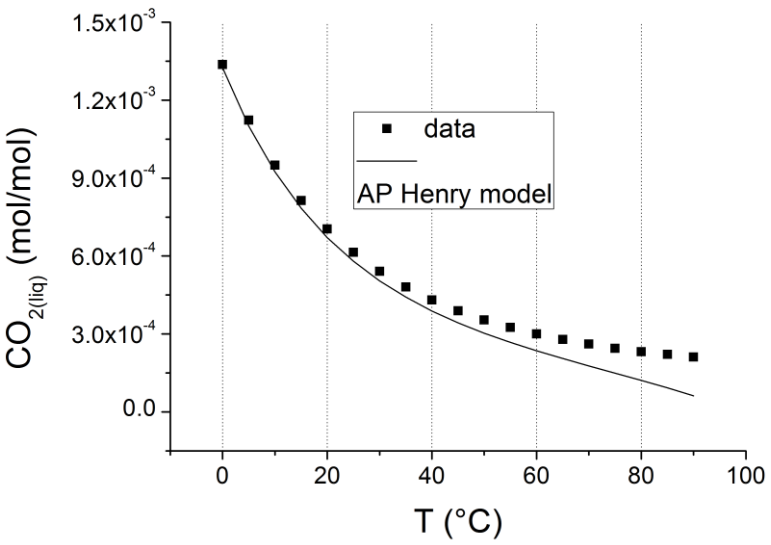

Figure 5: Solubility of CO_2 in water at increasing pressure.

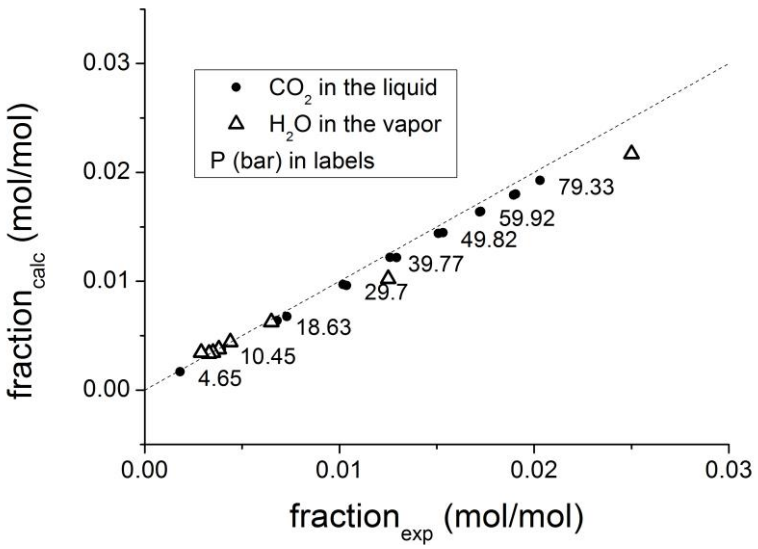

Figure 6: Solubility of H_2 in water at atmospheric pressure.

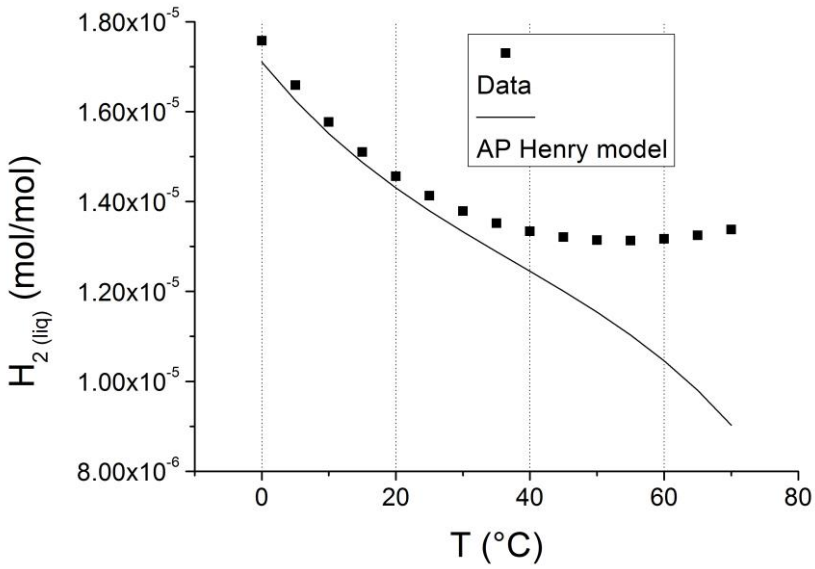

Figure 7: Solubility of H_2 in water at increasing pressure.

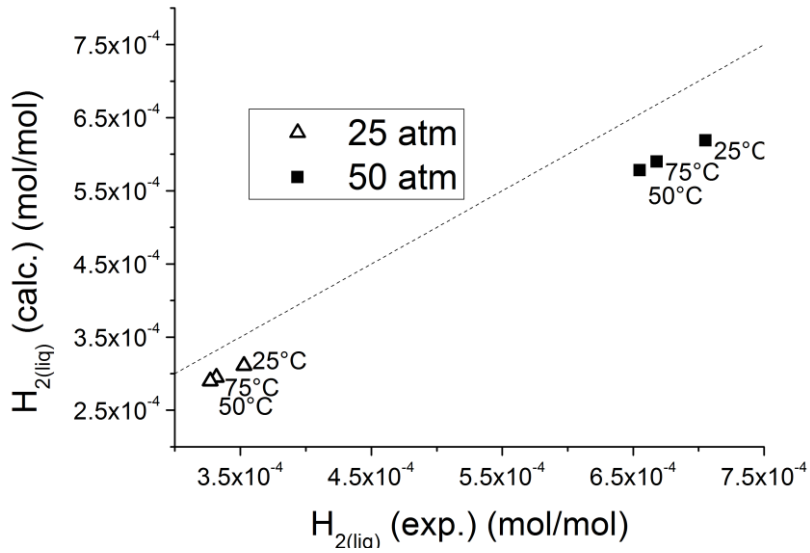

Figure 8: Capability of the APV9 database to reproduce the CO_2-K_2CO_3-H_2O system behavior (salt: 1% wt).

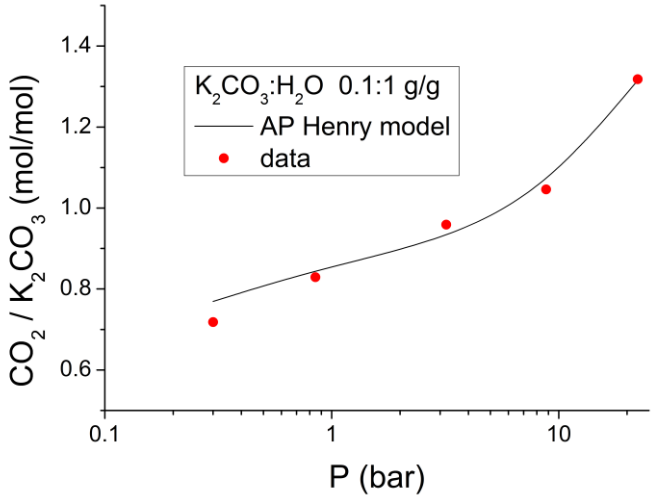

Figure 9: Capability of the APV9 database to reproduce the CO_2-K_2CO_3-H_2O system behavior (salt: 5% wt).

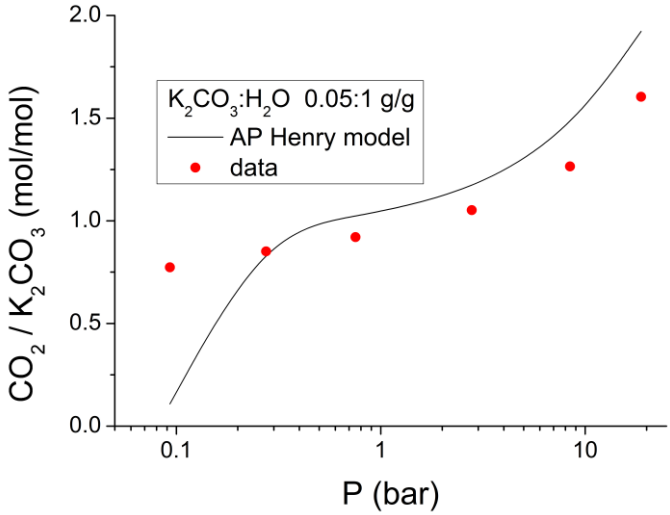

Figure 10: Calculated vs. experimental partial pressure of methane over saturated K_2CO_3 solutions.

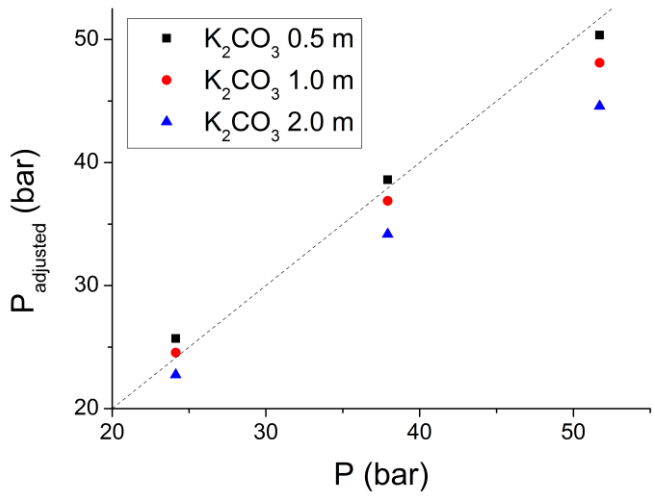

Figure 11: Parity plot for the hydrogen-methane vapor/liquid equilibrium (VLE).

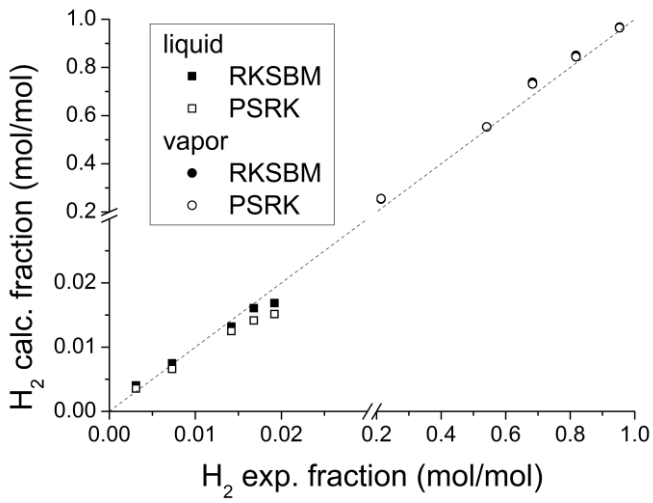

The gas solubility into water has been considered also above the atmospheric pressure because both the water separation and the CO_2 absorption take place in the 15-20 atm range. The adsorption equilibria of methane and water on one commercially available porous solid (Ba-loaded X zeolite) are reviewed in Figure 12 and 13, where the data from [45] and [46] are regressed to two simple Langmuir isotherms as in equations (11) and (12), at the temperature of 20°C and 25°C, respectively. Since the reviewed papers do not report multiple adsorption isotherms, it was not possible to retro-fit the parameters dependence on temperature, but this aspect has a little impact because the adsorption process was simulated at 25 °C. The Aspen Adsorption® built-in calculations require the partial pressure as basis, so at very high pressures there may be a mismatch when parameters

regressed from experimental fugacity are used, as in the present case: nevertheless, also in this case the process highest pressure is low enough to limit the non-ideality effects.

$$w_{CH_4}\left[\frac{kmol}{kg}\right] = \frac{0.001\left[\frac{kmol/kg}{bar}\right]P_{CH_4}}{1+2.2\left[\frac{kmol/kg}{bar}\right]P_{CH_4}} \qquad (11)$$

$$w_{H_2O}\left[\frac{kmol}{kg}\right] = \frac{3.5\left[\frac{kmol/kg}{bar}\right]P_{H_2O}}{1+2500\left[\frac{kmol/kg}{bar}\right]P_{H_2O}} \qquad (12)$$

Figure 12: Adsorption of methane on Ba-loaded zeolite.

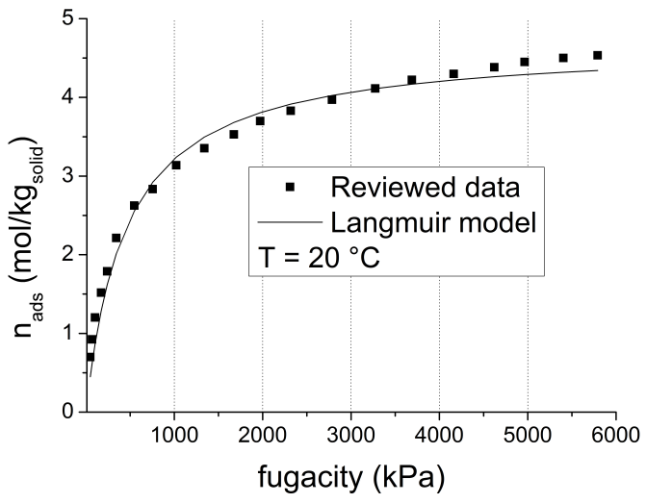

Figure 13: Adsorption of water on the same Ba-loaded zeolite.

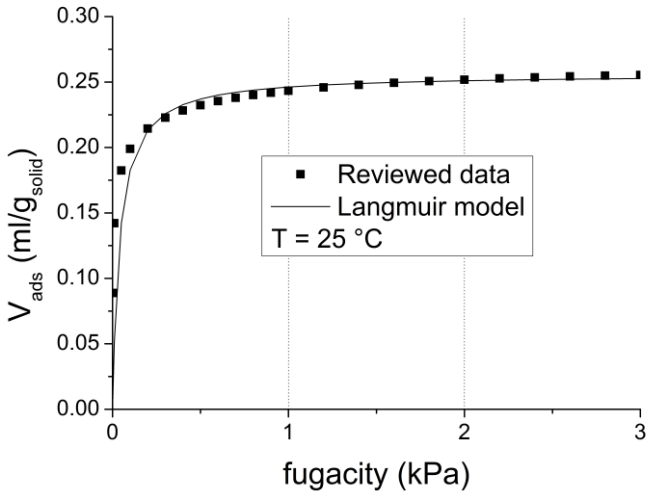

3. Results

3.1 Reactive Section

The thermodynamic models were selected and used following the dedicated guidelines [47]. As reviewed in Figures 2-11, the capability of the software databank to reproduce the available laboratory data is good: this test is essential and its good outcome assures the reliability of the simulation results, within the experimental ranges in which they were validated.

The full process layout is reported in Figure 14, where the thicker lines represent the main process streams. The operating conditions of each block are variable as for T and P and are described within the text when needed. The data be retrieved in all the Stream Tables reported in the Appendix, relative to the optimized case. The multi-stage reactor has been modeled using multiple, multi-tubular Plug-Flow Reactor blocks [23], adjusting the catalyst density and particle size in order to get reasonable pressure drops [48]. The first stage is calculated with equation (4) and is not followed by a cooling stage, so it acts as a "starter" for the reactor. The following four stages are designed to convert 75% of the CO_2: the product is cooled after each stage (detailed scheme in Figure 15) and the reactive bed itself is represented as a bundle of tubes packed with the catalyst and cooled by the feed flowing shell-side. The thermal profile is detailed in Figure 16. A comparative calculation supposing adiabatic beds with inter-coolers (Figure 17) shows that both approaches are possible, but cooling the reactive zones reduces the maximal temperature reached and saves 340 kW_{th} per ton of fresh CO_2.

Figure 14: Detailed layout of the plant.

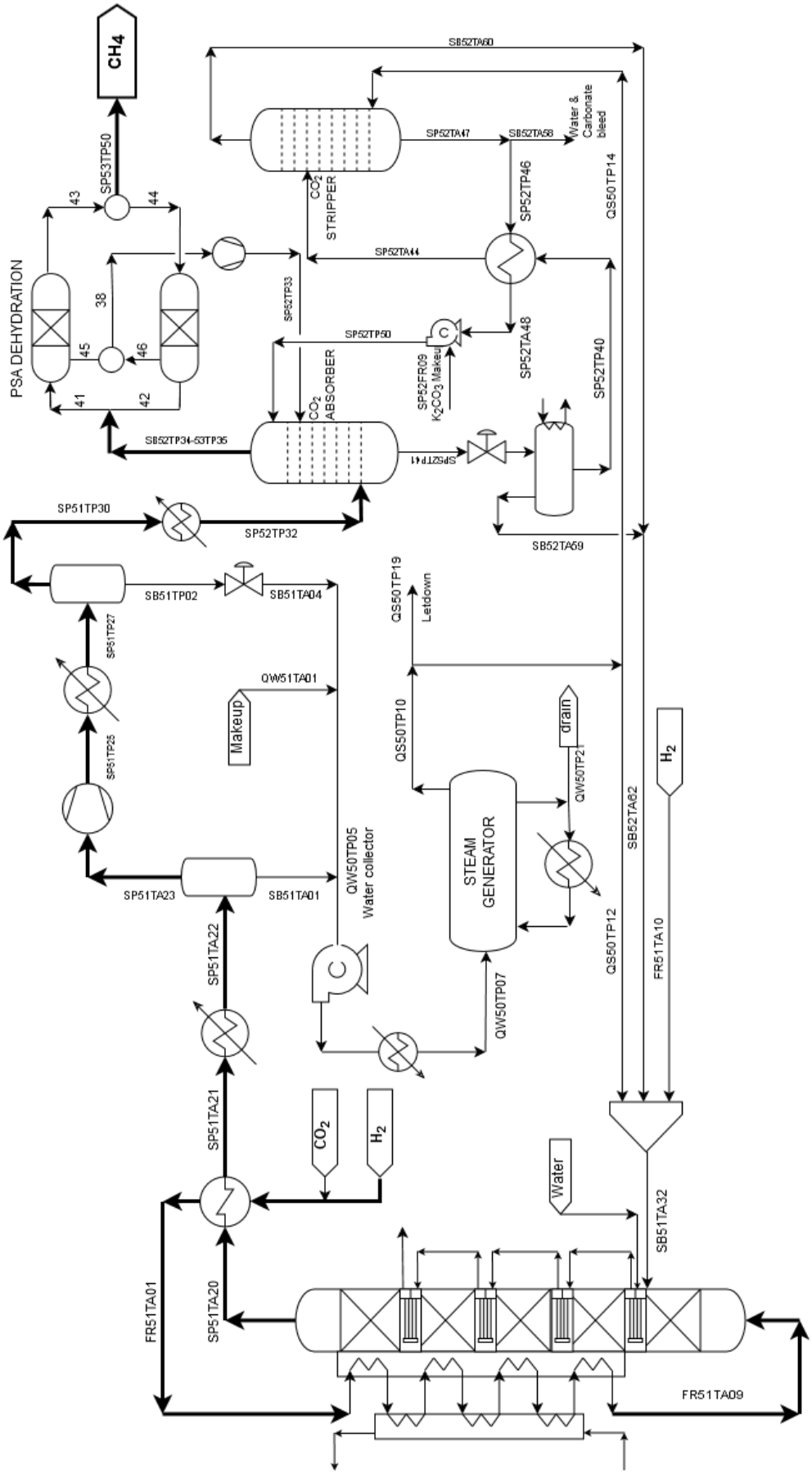

Figure 15: Detail of the reactor stages cooling.

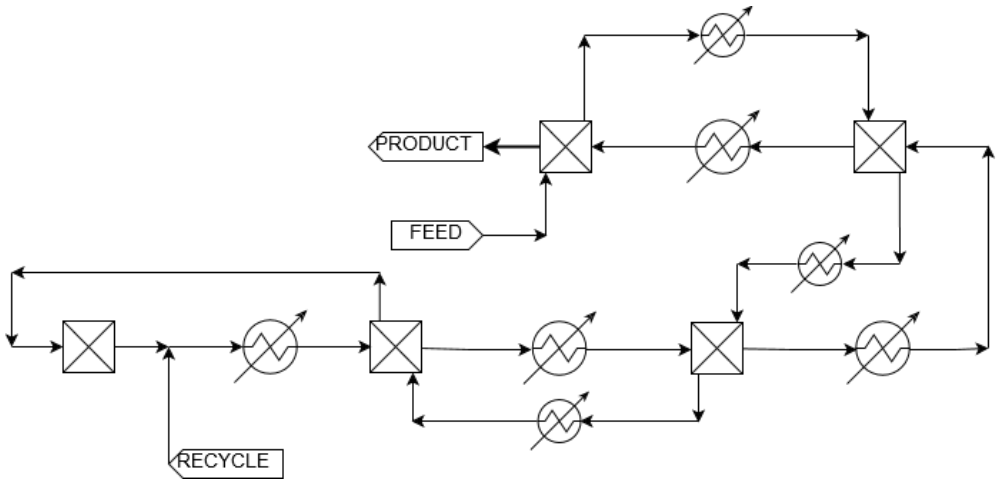

Figure 16: Conversion-temperature profile of the reactor (circlets) compared to the equilibrium condition for the given feed.

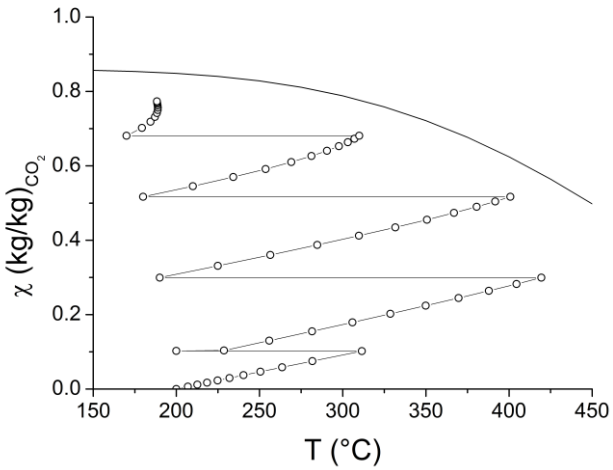

Figure 17: Comparison of temperature and conversion between the cooled stages (second to fifth) and a similar array of adiabatic ones.

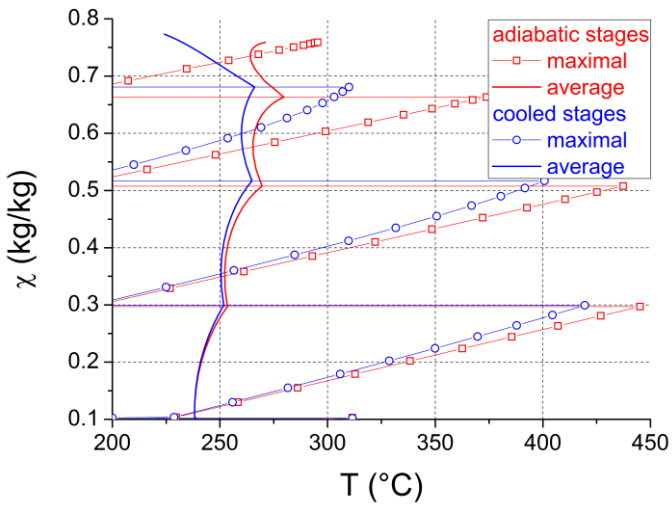

3.2 Recycle Section

The water present in the product stream yields a relatively high dew-point calculation, so the first condensation can be done at 80 °C; the following compression (see detailed process scheme in Figure 14) is actually split in four stages with inter-cooling (using the 'multi-stage' option within the Compressor block), at constant pressure ratios up to 17 bars. This pressure lets operate the second water dump still above 70 °C, and determines also the condition for the CO_2 adsorption in the scrubbing solvent: even if lower total pressures could be considered for this stage [49,50], it is convenient to maintain the gas pressurized for the further PSA section (the potassium process is anyway quite flexible from this point of view and still higher pressure can be employed [41]).

After being reboiled, part of the process water is injected directly into the reactor as LP steam. Most of this current is used to strip the carbon dioxide from the spent potassium bicarbonate solution leaving the absorber to regenerate fresh potassium carbonate. Then the water-saturated CO_2 gas constitute the main reactor recycle. The lean solvent is a 9% g/g solution of K_2CO_3, assuring a loading of 2.1 mol_{K^+}/mol_{CO_2} and 0.2% kg/kg of residue CO_2. In this work, where the overall process balances are the main interest, the absorber and the stripper are both simulated as tray columns where each stage is at thermodynamic equilibrium.

3.3 Pressure-Swing Adsorption

The PSA section is simulated straightforwardly as two solid beds (scheme in Figure 18) switched by a 4-step cycle. Unfortunately, the cited adsorption data do not provide any dynamic information such as the diffusion coefficients of the molecules into the solid pores. Nevertheless, an estimate of the ratio D_p/r for methane on a similar zeolite can be found in [51] and the value has been rescaled following the general considerations of Nakao and Suzuki [52], finding a range of 2 – 3 s^{-1} according to other simulation details that, anyway, can differ by the experimental parameters reviewed. So, it has to be pointed out that the used mass transfer coefficient is tentative, and more refined calculations will have to complete this aspect of the design. The other parameters (bed size, packing) are chosen in order to have low pressure drops (these are calculated automatically by the Aspen Adsorption® package using the Karman-Kozeny correlation).

The bed working/purge time was chosen after a preliminary evaluation of the water breakthrough out of an initially dry solid, and the load/unload step duration depends directly on the bed volumes under the chosen high and low pressures (Table 2).

Figure 18: Scheme of the PSA calculation with Aspen Adsorption®.

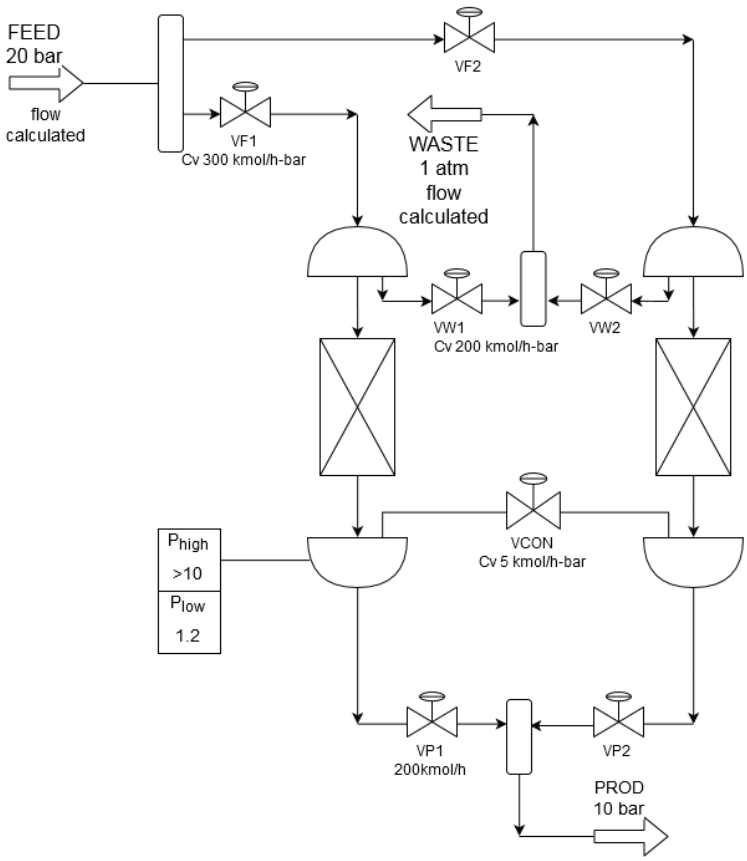

Figure 19: Transient profiles of the water fraction decrease in the synthetic gas product.

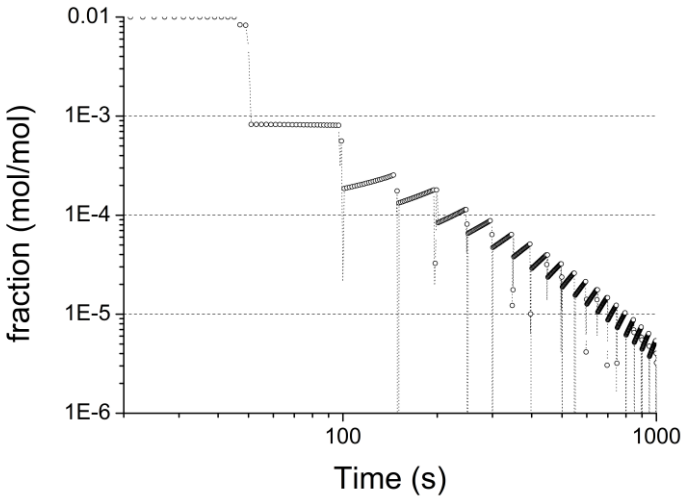

Figure 19 shows how the system reaches a steady state with a substantially decreased water content in the product. One third of the dry methane is used to purge water from the offline bed and is recycled to the CO_2 absorber, so the methane flow through the purification sections is actually 150% of the nominal plant product, as the CO_2-CH_4 molar flow through the reactor is the 125%.

Table 2: PSA specifications. 'Cv' means that the valve returns a linearized pressure drop ΔP=Cv×Flow; 'Flow' means that the valve maintains a fixed flowrate for any pressure drop across it. Valves names as in Figure 18.

General specifications			
Parameter	**Value**	**Units**	**Description**
Bed height	0.5	m	
Bed diameter	0.4	m	
ε	0.5	m^3/m^3	Inter-particle voidage
ε_p	0.7	m^3/m^3	Intra-particle voidage
ρ	1920	kg/m^3	Adsorbent density
r_p	0.001	m	Adsorbent particle radius
MTC	1 – 10	1/s	Lumped mass transfer coefficient

Valves Cycle schedule								
Step	**duration (s)**	**VCON**	**VF1**	**VF2**	**VP1**	**VP2**	**VW1**	**VW2**
1	45	Cv	Full open	Closed	Flow	Closed	Closed	Cv

2	5	Closed	Closed	Cv	Closed	Closed	Cv	Closed
3	45	Cv	Closed	Full open	Closed	Flow	Cv	Closed
4	5	Closed	Cv	Closed	Closed	Closed	Closed	Cv

3.4 Global balance and Energy Recovery

The detail of all the operating conditions and streams are reported in the Appendix, Tables 3-10.

The ratio between the chemical species present through the main line is showed in Figure 20, for a nominal methane yield of 200 kmol/h (107,000 Nm^3/day) and a complete CO_2 conversion. Performing the calculation in detail, the hydrogen fed to the reactor has been adjusted to a slight excess with respect to the reference value of C:H=1:8 mol/mol ratio, but its possible adsorption within the PSA beds alongside methane has been neglected, due to the facts that: i) on most zeolites, methane is adsorbed preferentially with respect to hydrogen [51], ii) the partial pressure of hydrogen is much lower than that of methane; as a result, the output stream can contain up to 3% mol/mol (0.4% wt) of unreacted hydrogen.

Figure 20: Composition of the gas outflowing the main process sections.

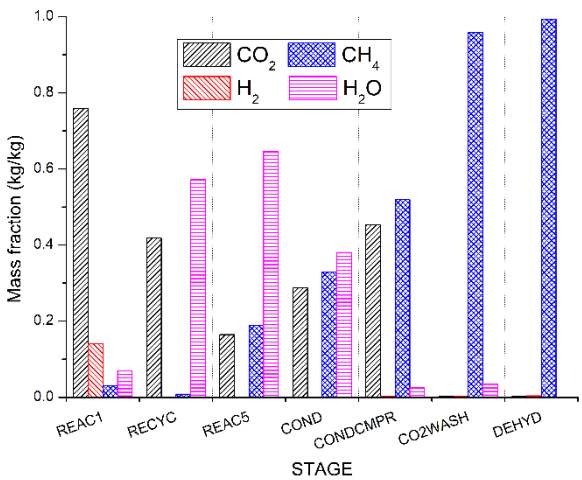

The energy balances are reported through the fluid list in **Table *10*** (names are relative to the scheme in Figure 14). This list constitutes also the first input for the basic pinch analysis of the flowsheet (performed with a custom Matlab routine based on the code distributed by MathWorks [53], with a rather conservative global ΔT_{min}=10 °C), whose results are in Figure 21 and Figure 22. The reaction heat can theoretically supply all the heat needed to bring a supposedly cold feed up in the 180-220 °C range needed to overcome the activation

energy, plus the heat to reboil the process condensate and recycle it to the stripper and the reactor, so the analysis yields a threshold problem [54] and the pinch point has to be located at about 100 °C.

Figure 21: Process composite curves (HCC: Hot Composite Curve; CCC: Cold Composite Curve).

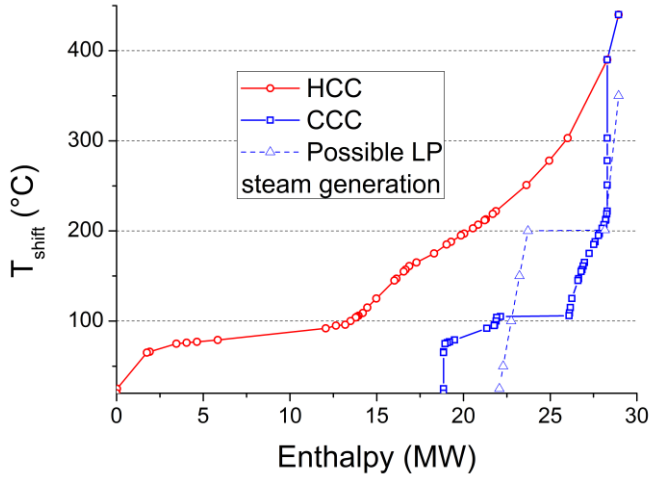

Figure 22: Process and process + utility Grand Composite Curves.

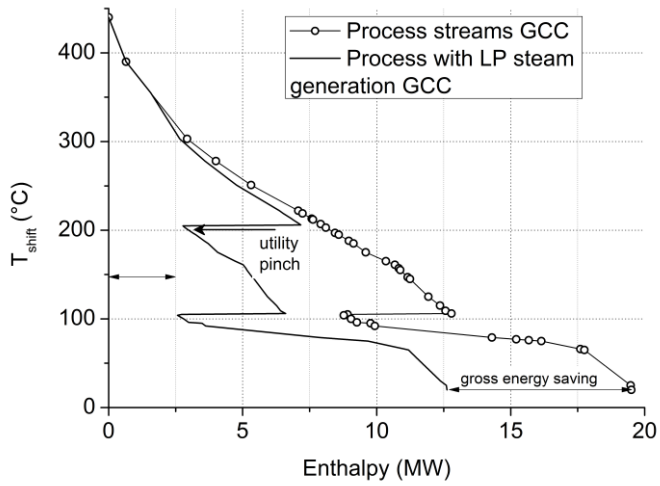

The thermal energy that can be recovered depends on the choice between two options: i) between 100 and 110 °C there are at least 12 MW available, in principle, for waste-heat utilizers as co-generation networks [55,56]; ii) 7-8 MW can be used at the 200 °C level to rise LP steam. In any case, the heat released to the cold sink cannot be reduced below 9 MW (*i.e.* the position of the process pinch).

Notice that the compression power is calculated to be 1.8 MW (at 90% isentropic efficiency) and the pumping between the adsorption and the stripper plus the PSA-waste recompression make up for 2.2 MW_{el} in total. In

principle, this power could be provided by the above foreseen LP steam generation via a Rankine bottoming cycle with an efficiency of 31% [57].

3.5 Downstream Treatment

The residual hydrogen can be removed designing in more detail a better-performing PSA section. In this case, alternative process options may open, according to the methane flow used as purge stream and to its hydrogen tenor (namely, recycle to the reactor or use as fuel).

Nevertheless, a hydrogen fraction as low as 3% vol does not prevent the synthetic gas to be injected into the up-to-date methane network [58], or for the straightforward 'dilution' and use of renewable hydrogen [59]: in the power-to-gas framework this choice would indeed be very promising.

In view of the possible use of the synthetic gas at sites far from the production one (that in turn should be better placed where renewable hydrogen is available), also a liquefaction process is considered (scheme and result in Figure 23-25), calculating a Conoco-Philips process [60] based on propylene, ethylene and pure methane (comparison data from [61]) with the following modification: the SNG pressure downstream the PSA is maintained though all the refrigeration heat exchangers, until the final expansion into a liquid-vapor separator from where the residual hydrogen (13 kg/h) is released together with the methane vapor in equilibrium at -163 °C (507 kg/h, *i.e.* 13% of the rated yield).

Figure 23: Scheme of the cryogenic train simulated, each stage being a dual-pressure refrigeration cycle. Only the propylene heat dissipator downstream the compression releases heat to the external cold sink.

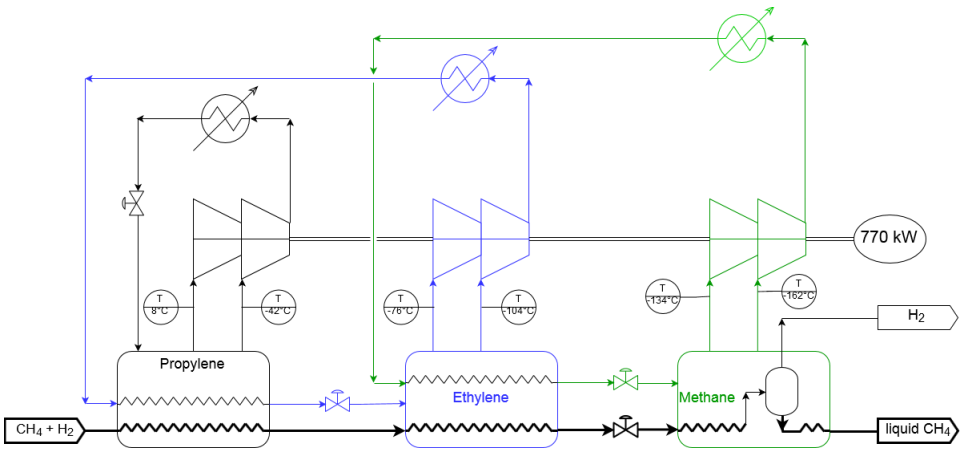

Figure 24: Thermal cascade of the cryogenic section.

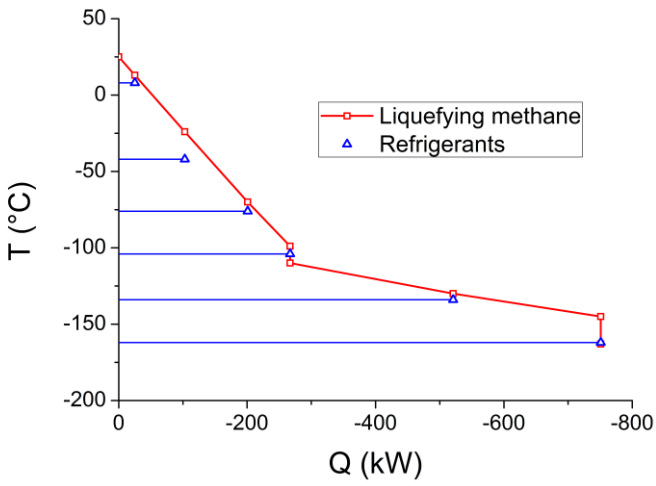

Figure 25: Temperature-duty diagram of the cryogenic section.

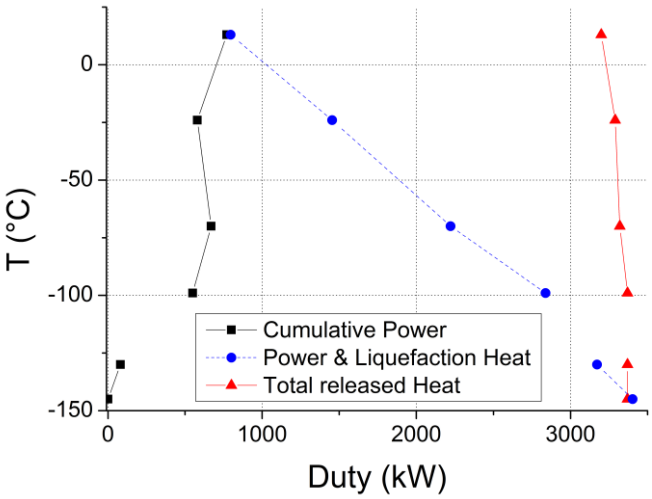

4. Conclusions

The experimental tests and mathematical formulations found in the literature for the CO and CO_2 methanation have been constantly increased in number and quality, building a sound background for the choice of catalysts and models for a reliable process design. The exothermal character of the reaction has already been addressed in detailed reactor calculations, while overall plant balances mostly rely on simplified equilibrium yields.

In this work two detailed reaction kinetics are linked to a full-scale plant simulation, thus getting a clearer picture of the actual performance of the whole plant, to assess its feasibility, besides of the thermal management

of the reactor, of the temperature range available for thermal recoveries and of the impact of the purification solutions. The main findings can be summarized as follows:

1. Without removing water (or methane), at least 4 reactive stages are foreseen to achieve conversions higher than 75% (on a mass basis);
2. catalysts with a lower activation energy let operate the last reaction stages in conditions more favorable from a thermodynamic point of view: in this case, the process can be operated at atmospheric pressure, with considerable improvement of the safety and cost of the plant;
3. both adiabatic or cooled reactive beds are viable, the second option looks more attractive but the best solution will depend on the detailed solutions of the reactor internals and dynamic control;
4. all the reactor stages can be operated with recycled CO_2 and water with limited energy penalties, because the process steam requires less than 5 MW out of the 13 available above 100 °C, so this option represents mainly a capital cost;
5. waste-heat utilizers can recover most of the available thermal energy, while steam generation becomes less important as its pressure (and quality) is increased (shape of the GCC in Figure 22);
6. the reactor has to grant a complete conversion of the fresh CO_2, but hydrogen in the product stream can be foreseen according to the eventual use of the gas, making the process all the more flexible.
7. in summary, the foreseen temperature range for this reaction does not exceed 400 °C, and the pressure must not be necessarily increased before the separation stages; gas-to-gas cooling of the reactive beds are a good compromise between adiabatic stages (prone to hot-spots development) and direct steam generation (that requires a more expensive pressurized shell).

The developed concept presents, in principle, multiple solutions sensibly different from the point of view of the capital and operative costs, so its scale has been initially set to a medium size.

The right size of the process will depend, anyway, on the available quantity of renewable hydrogen (or energy), and on the market price of the SNG for the given combination of producers/distribution/customers at that level, so the best detail solutions (regarding mass and energy recycles, catalyst per-pass conversion, PSA beds, etc.) will be designed accordingly.

Symbols

h	specific enthalpy	E	activation energy
n	moles reacting	K	equilibrium constant
r	reaction rate	P	pressure
u	velocity normalized for catalyst load	R	gas constant
z	axial reactor coordinate	T	temperature
ν	stoichiometric coefficient	U	heat transfer coefficient

Bibliography

(1) Jacobson, M. Z. *Evaluation of Coal and Natural Gas With Carbon Capture as Proposed Solutions to Global Warming, Air Pollution, and Energy Security*. **2019**.

(2) Collet, P.; Flottes, E.; Favre, A.; Raynal, L.; Pierre, H.; Capela, S.; Peregrina, C. *Techno-Economic and Life Cycle Assessment of Methane Production via Biogas Upgrading and Power to Gas Technology*. *Appl. Energy* **2017**, *192*, 282–295. https://doi.org/10.1016/j.apenergy.2016.08.181.

(3) Rönsch, S.; Schneider, J.; Matthischke, S.; Schlüter, M.; Götz, M.; Lefebvre, J.; Prabhakaran, P.; Bajohr, S. *Review on Methanation - From Fundamentals to Current Projects*. *Fuel* **2016**, *166*, 276–296. https://doi.org/10.1016/j.fuel.2015.10.111.

(4) Dincer, I.; Acar, C. *Review and Evaluation of Hydrogen Production Methods for Better Sustainability*. *Int. J. Hydrogen Energy* **2014**, *40* (34), 11094–11111. https://doi.org/10.1016/j.ijhydene.2014.12.035.

(5) Bakhtyari, A.; Makarem, M. A.; Rahimpour, M. R. *Hydrogen Production Through Pyrolysis*. In *Encyclopedia of Sustainability Science and Technology.*; (Eds.), M. R., Ed.; Springer, New York, NY., 2018. https://doi.org/https://doi.org/10.1007/978-1-4939-2493-6.

(6) Buchholz, O. S.; Van Der Ham, A. G. J.; Veneman, R.; Brilman, D. W. F.; Kersten, S. R. A. *Power-to-Gas: Storing Surplus Electrical Energy a Design Study*. *Energy Procedia* **2014**, *63*, 7993–8009. https://doi.org/10.1016/j.egypro.2014.11.836.

(7) Baier, J.; Schneider, G.; Heel, A. *A Cost Estimation for CO2 Reduction and Reuse by Methanation from Cement Industry Sources in Switzerland*. *Front. Energy Res.* **2018**, *6* (FEB), 1–9. https://doi.org/10.3389/fenrg.2018.00005.

(8) Norhasyima; Mahliaa. *Advances in CO_2 Utilization Technology: A Patent Landscape Review*. *J. CO2 Util.* **2018**, *26*, 323–335.

(9) Rieke, S. *Solar Fuels and Power-to-Gas Technologies*; Lyon, 2012.

(10) Götz, M.; Lefebvre, J.; Mörs, F.; McDaniel Koch, A.; Graf, F.; Bajohr, S.; Reimert, R.; Kolb, T. *Renewable Power-to-Gas: A Technological and Economic Review*. *Renew. Energy* **2016**, *85*, 1371–1390. https://doi.org/10.1016/j.renene.2015.07.066.

(11) Bailera, M.; Lisbona, P.; Romeo, L. M.; Espatolero, S. *Power to Gas Projects Review: Lab, Pilot and Demo Plants for Storing Renewable Energy and CO2*. *Renew. Sustain. Energy Rev.* **2017**, *69* (October 2016), 292–312. https://doi.org/10.1016/j.rser.2016.11.130.

(12) Beaudin, M.; Zareipour, H.; Schellenberglabe, A.; Rosehart, W. *Energy Storage for Mitigating the Variability of Renewable Electricity Sources: An Updated Review*. *Energy Sustain. Dev.* **2010**, *14* (4), 302–314. https://doi.org/10.1016/j.esd.2010.09.007.

(13) Prakash Parthasarathy, K. S. N. *Hydrogen Production from Steam Gasification of Biomass: Influence Ofprocess Parameters on Hydrogen YieldeA Review*. *Renew. Energy* **2014**, *66*, 570–579.

(14) Fujita, S. I.; Takezawa, N. *Difference in the Selectivity of CO and CO2 Methanation Reactions*. *Chem. Eng. J.* **1997**, *68* (1), 63–68. https://doi.org/10.1016/S1385-8947(97)00074-0.

(15) Duyar, M. S.; Ramachandran, A.; Wang, C.; Farrauto, R. J. *Kinetics of CO2 Methanation over Ru/γ-Al2O3 and Implications for Renewable Energy Storage Applications*. *J. CO2 Util.* **2015**, *12*, 27–33. https://doi.org/10.1016/j.jcou.2015.10.003.

(16) Brooks, K. P.; Hu, J.; Zhu, H.; Kee, R. J. *Methanation of Carbon Dioxide by Hydrogen Reduction Using the Sabatier Process in Microchannel Reactors*. *Chem. Eng. Sci.* **2007**, *62* (4), 1161–1170. https://doi.org/10.1016/j.ces.2006.11.020.

(17) Karelovic, A.; Ruiz, P. *Mechanistic Study of Low Temperature CO2 Methanation over Rh/TiO2 Catalysts*. *J. Catal.* **2013**, *301*, 141–153. https://doi.org/10.1016/j.jcat.2013.02.009.

(18) Abelló, S.; Berrueco, C.; Montané, D. *High-Loaded Nickel–Alumina Catalyst for Direct CO2 Hydrogenation into Synthetic Natural Gas (SNG)*. *Fuel* **2013**, *113*, 598–609. https://doi.org/10.1016/J.FUEL.2013.06.012.

(19) Tada, S.; Shimizu, T.; Kameyama, H.; Haneda, T.; Kikuchi, R. *Ni/CeO2 Catalysts with High CO2*

Methanation Activity and High CH4 Selectivity at Low Temperatures. *Int. J. Hydrogen Energy* **2012**, *37* (7), 5527–5531. https://doi.org/10.1016/j.ijhydene.2011.12.122.

(20) Görke, O.; Pfeifer, P.; Schubert, K. *Highly Selective Methanation by the Use of a Microchannel Reactor*. *Catal. Today* **2005**, *110* (1–2), 132–139. https://doi.org/10.1016/j.cattod.2005.09.009.

(21) Ghaib, K.; Nitz, K.; Ben-Fares, F.-Z. *Chemical Methanation of CO 2 : A Review* . *ChemBioEng Rev.* **2016**, *3* (6), 266–275. https://doi.org/10.1002/cben.201600022.

(22) ISTAT. Consumo procapite di gas metano per uso domestico e riscaldamento.

(23) Jürgensen, L.; Ehimen, E. A.; Born, J.; Holm-Nielsen, J. B. *Dynamic Biogas Upgrading Based on the Sabatier Process: Thermodynamic and Dynamic Process Simulation*. *Bioresour. Technol.* **2015**, *178*, 323–329. https://doi.org/10.1016/j.biortech.2014.10.069.

(24) Rönsch, S.; Köchermann, J.; Schneider, J.; Matthischke, S. *Global Reaction Kinetics of CO and CO2 Methanation for Dynamic Process Modeling*. *Chem. Eng. Technol.* **2016**, *39* (2), 208–218. https://doi.org/10.1002/ceat.201500327.

(25) Sun, D.; Khan, F. M.; Simakov, D. S. A. *Heat Removal and Catalyst Deactivation in a Sabatier Reactor for Chemical Fixation of CO2: Simulation-Based Analysis*. *Chem. Eng. J.* **2017**, *329*, 165–177. https://doi.org/10.1016/j.cej.2017.06.160.

(26) Hoekman, S. K.; Broch, A.; Robbins, C.; Purcell, R. *CO2 Recycling by Reaction with Renewably-Generated Hydrogen*. *Int. J. Greenh. Gas Control* **2010**, *4* (1), 44–50. https://doi.org/10.1016/j.ijggc.2009.09.012.

(27) Schaaf, T.; Grünig, J.; Schuster, M.; Orth, A. *Speicherung von Elektrischer Energie Im Erdgasnetz - Methanisierung von CO2-Haltigen Gasen*. *Chemie-Ingenieur-Technik* **2014**, *86* (4), 476–485. https://doi.org/10.1002/cite.201300144.

(28) Stolaroff, J. K. *Carbonate Solutions for Carbon Capture : A Summary*; Livermore, CA, 2013.

(29) Milidovich, S.; Zbacnik, E. *Increasing Efficiency of Hot Potassium Carbonate CO 2 Removal Systems*; 2013.

(30) Lazdans, A.; Dace, E.; Gusca, J. *Development of the Experimental Scheme for Methanation Process*. *Energy Procedia* **2016**, *95*, 540–545. https://doi.org/10.1016/j.egypro.2016.09.082.

(31) Müller, K.; Fleige, M.; Rachow, F.; Schmeißer, D. *Sabatier Based CO2-Methanation of Flue Gas*

Emitted by Conventional Power Plants. *Energy Procedia* **2013**, *40*, 240–248. https://doi.org/10.1016/j.egypro.2013.08.028.

(32) Hashimoto, K.; Yamasaki, M.; Meguro, S.; Sasaki, T.; Katagiri, H.; Izumiya, K.; Kumagai, N.; Habazaki, H.; Akiyama, E.; Asami, K. *Materials for Global Carbon Dioxide Recycling*. *Corros. Sci.* **2002**, *44* (2), 371–386. https://doi.org/10.1016/S0010-938X(01)00067-1.

(33) Rufford, T. E.; Smart, S.; Watson, G. C. Y.; Graham, B. F.; Boxall, J.; Diniz da Costa, J. C.; May, E. F. *The Removal of CO2 and N2 from Natural Gas: A Review of Conventional and Emerging Process Technologies*. *J. Pet. Sci. Eng.* **2012**, *94–95*, 123–154. https://doi.org/10.1016/j.petrol.2012.06.016.

(34) Chapel, D. G.; Mariz, C. L.; Ernest, J. *Recovery of CO2 from Flue Gases: Commercial Trends*; Saskatoon, Saskatchewan, Canada, 1999.

(35) Sander, R. *Compilation of Henry's Law Constants (Version 4.0) for Water as Solvent*. *Atmos. Chem. Phys.* **2015**, *15* (8), 4399–4981. https://doi.org/10.5194/acp-15-4399-2015.

(36) *IUPAC Solubility Data Series - Methane, Volume 27/28*; Young, C. L., Clever, H. L., Eds.; 1987.

(37) Wilhelm, E.; Battino, R.; Wilcock, R. J. *Low-Pressure Solubility of Gases in Liquid Water*. *Chem. Rev.* **1977**, *77* (2), 219–262. https://doi.org/10.1021/cr60306a003.

(38) Valtz, A.; Chapoy, A.; Coquelet, C.; Paricaud, P.; Richon, D. *Vapour-Liquid Equilibria in the Carbon Dioxide-Water System, Measurement and Modelling from 278.2 to 318.2 K*. *Fluid Phase Equilib.* **2004**, *226* (1–2), 333–344. https://doi.org/10.1016/j.fluid.2004.10.013.

(39) Crovetto, R.; Fernández-Prini, R.; Japas, M. L. *Solubilities of Inert Gases and Methane in H2O and in D 2O in the Temperature Range of 300 to 600 K*. *J. Chem. Phys.* **1982**, *76* (2), 1077–1086. https://doi.org/10.1063/1.443074.

(40) Young, C. L. *IUPAC Solubility Data Series: Hydrogen and Deuterium*; 1981; Vol. 5/6. https://doi.org/10.1016/0021-9614(80)90193-7.

(41) Ochieng, R.; Berrouk, A.; Peters, C. J. *Simulation of the Benfield HiPure Process of Natural Gas Sweetening for LNG Production and Evaluation of Alternatives*. 1–18.

(42) Pérez-Salado Kamps, Á.; Meyer, E.; Rumpf, B.; Maurer, G. *Solubility of CO_2 in Aqueous Solutions of KCl and in Aqueous Solutions of K_2CO_3*. *J. Chem. Eng. Data* **2007**, *52* (3), 817–832. https://doi.org/10.1021/je060430q.

(43) Stoessell, R. K.; Byrne, P. A. *Salting-out of Methane in Single-Salt Solutions at 25°C and below 800 Psia*. *Geochim. Cosmochim. Acta* **1982**, *46* (8), 1327–1332. https://doi.org/10.1016/0016-7037(82)90268-X.

(44) Sagara, H.; Arai, Y.; Saito, S. *Vapor-Liquid Equilibria of Binary and Ternary Systems Containing Hydrogen and Light Hydrocarbons*. *J. Chem. Eng. Japan* **1972**, *5* (4), 339–348. https://doi.org/10.1252/jcej.5.339.

(45) Zhang, S.; Talu, O.; Hayhurst, D. T. *High-Pressure Adsorption of Methane in NaX, MgX, CaX, SrX, and BaX*. *J. Phys. Chem.* **1991**, *40* (95), 1722–1726.

(46) Moise, J. C.; Bellat, J. P.; Méthivier, A. *Adsorption of Water Vapor on X and Y Zeolites Exchanged with Barium*. *Microporous Mesoporous Mater.* **2001**, *43* (1), 91–101. https://doi.org/10.1016/S1387-1811(00)00352-8.

(47) Sandler, S. I. *Using Aspen Plus in Thermodynamic Instruction*; American Institute of Chemical Engineers - Wiley & Sons: Hoboken, New Jersey, 2015.

(48) Kiewidt, L.; Thöming, J. *Predicting Optimal Temperature Profiles in Single-Stage Fixed-Bed Reactors for CO2-Methanation*. *Chem. Eng. Sci.* **2015**, *132*, 59–71. https://doi.org/10.1016/j.ces.2015.03.068.

(49) Yildirim, Ö.; Kiss, A. A.; Hüser, N.; Leßmann, K.; Kenig, E. Y. *Reactive Absorption in Chemical Process Industry: A Review on Current Activities*. *Chem. Eng. J.* **2012**, *213*, 371–391. https://doi.org/10.1016/j.cej.2012.09.121.

(50) Thee, H.; Suryaputradinata, Y. A.; Mumford, K. A.; Smith, K. H.; Silva, G. da; Kentish, S. E.; Stevens, G. W. *A Kinetic and Process Modeling Study of CO 2 Capture with MEA-Promoted Potassium Carbonate Solutions*. *Chem. Eng. J.* **2012**, *210*, 271–279. https://doi.org/10.1016/j.cej.2012.08.092.

(51) Delgado, J. A.; Águeda, V. I.; Uguina, M. A.; Sotelo, J. L.; Brea, P.; Carlos, A.; Grande, C. A. *Adsorption and Diffusion of H2, CO, CH4, and CO2 in BPL Activated Carbon and 13X Zeolite: Evaluation of Performance in Pressure Swing Adsorption Hydrogen Purification by Simulation*. *Ind. Eng. Chem. Res.* **2014**, *53* (40), 15414–15426. https://doi.org/10.1021/ie403744u.

(52) Nakao, S. I.; Suzuki, M. *Mass Transfer Coefficient in Cyclic Adsorption and Desorption*. *J. Chem. Eng. Japan* **1983**, *16* (2), 114–119. https://doi.org/10.1252/jcej.16.114.

(53) Matteo Morandin. cascade.m.

(54) Kemp, I. C. *Pinch Analysis and Process Integration: A User Guide on Process Integration for the Efficient Use of Energy*, 2nd ed.; Butterworth-Heinemann, an imprint of Elsevier: Linacre House, Jordan Hill, Oxford OX2 8DP, UK 30, 2007. https://doi.org/http://dx.doi.org/10.1016/B978-075068260-2.50003-1.

(55) Fang, H.; Xia, J.; Zhu, K.; Su, Y.; Jiang, Y. *Industrial Waste Heat Utilization for Low Temperature District Heating*. *Energy Policy* **2013**, *62*, 236–246. https://doi.org/10.1016/J.ENPOL.2013.06.104.

(56) Rosen, M. A.; Le, M. N.; Dincer, I. *Efficiency Analysis of a Cogeneration and District Energy System*. *Appl. Therm. Eng.* **2005**, *25* (1), 147–159. https://doi.org/10.1016/j.applthermaleng.2004.05.008.

(57) Petrov, M. P. *Steam Bottoming Cycles for the W20V34SG Gas Engine*; Stockholm, Sweden, 2006.

(58) Witkowski, A.; Rusin, A.; Majkut, M.; Stolecka, K. *Analysis of Compression and Transport of the Methane/Hydrogen Mixture in Existing Natural Gas Pipelines*. *Int. J. Press. Vessel. Pip.* **2018**, *166*, 24–34. https://doi.org/10.1016/j.ijpvp.2018.08.002.

(59) SNAM-McKinsey. *The Hydrogen Challenge: The Potential of Hydrogen in Italy*; 2019.

(60) Adolfo, D.; Carcasci, C.; Falchetti, C.; Lubello, P. *Thermo-Economic Analysis of a Natural Gas Liquefaction Plant*. *Energy Procedia* **2018**, *148*, 42–49. https://doi.org/10.1016/j.egypro.2018.08.017.

(61) Buhner, K.; Maurer, G.; Bender, E. *Pressure-Enthalpy Diagrams for Methane, Ethane, Propane, Ethylene and Propylene*. *Cryogenics (Guildf).* **1981**, *100* (March), 157–164.

Appendix

Stream reports

Table 3: Stream report of the feeds and reactor section.

Stream	FR51TA01	TR51TA10	TR51TA13	TR51TA15	TR51TA17	FR51TA09	FR51TA10	SP52FR09
Description								
Temp (°C)	60.00	309.89	444.51	395.48	307.57	200.00	80.00	25.00
Pres (bar)	1.30	1.17	1.16	1.15	1.12	1.20	1.30	1.10
Vapor (mol/mol)	1.00	1.00	1.00	1.00	1.00	1.00	1.00	0.00
MW (g/mol)	10.35	10.78	15.41	17.12	18.76	10.35	16.01	45.78
Mole Flow (kmol/h)	1008.00	967.58	1133.38	1020.15	931.07	1008.00	6.00	6.71
Mass Flows (kg/h)								
TOTAL	10430.79	10430.79	17464.24	17464.24	17464.24	10430.79	96.08	307.01
CARBO-01	8801.96	7912.53	7943.46	5451.90	3491.69	8801.96	88.02	0.00
HYDRO-01	1628.83	1465.87	940.97	484.47	125.31	1628.83	8.06	0.00
METHA-01	0.00	324.22	1443.80	2352.04	3066.59	0.00	0.00	0.00
WATER	0.00	728.17	7136.01	9175.83	10780.65	0.00	0.00	70.74
K^+	0.00	0.00	0.00	0.00	0.00	0.00	0.00	39.32
$K_2CO_{3(S)}$	0.00	0.00	0.00	0.00	0.00	0.00	0.00	160.39
$KHCO_{3(S)}$	0.00	0.00	0.00	0.00	0.00	0.00	0.00	7.33
OH^-	0.00	0.00	0.00	0.00	0.00	0.00	0.00	1.25
HCO_3^-	0.00	0.00	0.00	0.00	0.00	0.00	0.00	0.02
CO_3^{2-}	0.00	0.00	0.00	0.00	0.00	0.00	0.00	27.96
Mass Fractions								
CARBO-01	0.844	0.759	0.455	0.312	0.200	0.844	0.916	0.000
HYDRO-01	0.156	0.141	0.054	0.028	0.007	0.156	0.084	0.000
METHA-01	0.000	0.031	0.083	0.135	0.176	0.000	0.000	0.000
WATER	0.000	0.070	0.409	0.525	0.617	0.000	0.000	0.230
K^+	0.000	0.000	0.000	0.000	0.000	0.000	0.000	0.128
$K2CO_{3(S)}$	0.000	0.000	0.000	0.000	0.000	0.000	0.000	0.522
$KHCO_{3(S)}$	0.000	0.000	0.000	0.000	0.000	0.000	0.000	0.024
OH^-	0.000	0.000	0.000	0.000	0.000	0.000	0.000	0.004
HCO_3^-	0.000	0.000	0.000	0.000	0.000	0.000	0.000	0.000
CO_3^{2-}	0.000	0.000	0.000	0.000	0.000	0.000	0.000	0.091

Table 4: Stream report for the first separation section.

Stream Description	SP51TA20	SP51TA21	SP51TA22	SP51TA23	SP51TP25	SP51TP26	SP51TP30
Temp (°C)	165.78	97.03	80.00	79.80	200.00	160.00	80.00
Pres (bar)	1.09	1.09	1.09	1.09	17.00	17.00	17.00
Vapor (mol/mol)	1.00	1.00	0.54	1.00	1.00	0.92	1.00
MW (g/mol)	19.34	19.34	19.34	20.46	20.46	20.46	22.18
Mole Flows (kmol/h)	903.20	903.20	903.20	487.80	487.80	487.80	285.61
Mass Flows (kg/h)							
TOTAL	17464.24	17464.24	17464.24	9980.26	9980.26	9980.26	6333.68
CARBO-01	2878.46	2878.46	2878.46	2877.87	2877.87	2877.87	2870.72
HYDRO-01	12.96	12.96	12.96	12.96	12.96	12.96	12.96
METHA-01	3290.12	3290.12	3290.12	3290.08	3290.08	3290.08	3289.53
WATER	11282.69	11282.69	11282.69	3799.35	3799.35	3799.35	160.48
Mass fractions							
CARBO-01	0.16482	0.16482	0.16482	0.288356	0.288356	0.288356	0.453247
HYDRO-01	0.000742	0	0	0	0.001298	0.0013	0.002046
METHA-01	0	0	0	0	0.329659	0.33	0.51937
WATER	1	1	1	0	0.380687	0.381	0.025337

Table 5: Stream report for the separation section (continued).

Stream Description	SP52TP32	SP52TP33	SP52TP34	SP53TP35	SP52TP40	SP52TP41	SP52TA44
Temp (°C)	70.78	70.00	80.70	25.00	70.00	84.01	86.94
Pres (bar)	17.00	17.00	17.00	17.00	2.00	17.00	1.00
Vapor (mol/mol)	0.99	1.00	1.00	1.00	0.00	0.00	0.01
MW (g/mol)	22.18	15.66	15.71	15.64	19.48	19.52	19.45
Mole Flow (kmol/h)	285.61	69.98	285.93	277.87	5957.00	5971.51	5966.84
Mass Flow (kg/h)							
TOTAL	6333.68	1095.94	4492.23	4346.92	116041	116580	116041
CARBO-01	2870.72	2.32	9.26	9.26	293.47	666.59	726.22
HYDRO-01	12.96	4.24	16.97	16.97	0.01	0.23	0.01
METHA-01	3289.53	1077.10	4308.41	4308.41	2.00	58.22	2.00
WATER	160.48	12.28	157.59	12.28	102362	102378	102539
POTAS-01	0.00	0.00	0.00	0.00	0.00	0.00	0.00
$H3O^+$	0.00	0.00	0.00	0.00	0.00	0.00	0.00
K^+	0.00	0.00	0.00	0.00	5317.29	5317.29	5317.29
OH^-	0.00	0.00	0.00	0.00	0.04	0.04	0.31
HCO_3^-	0.00	0.00	0.00	0.00	7841.26	8025.67	6642.25
CO_3^{2-}	0.00	0.00	0.00	0.00	224.72	134.03	813.85
Mass Fraction							
CARBO-01	0.453	0.002	0.002	0.002	0.003	0.006	0.006
HYDRO-01	0.002	0.004	0.004	0.004	0.000	0.000	0.000
METHA-01	0.519	0.983	0.959	0.991	0.000	0.000	0.000
WATER	0.025	0.011	0.035	0.003	0.882	0.878	0.884

POTAS-01	0.000	0.000	0.000	0.000	0.000	0.000	0.000
$H3O^+$	0.000	0.000	0.000	0.000	0.000	0.000	0.000
K^+	0.000	0.000	0.000	0.000	0.046	0.046	0.046
OH^-	0.000	0.000	0.000	0.000	0.000	0.000	0.000
HCO_3^-	0.000	0.000	0.000	0.000	0.068	0.069	0.057
CO_3^{2-}	0.000	0.000	0.000	0.000	0.002	0.001	0.007

Table 6: Stream report for the separation section (continued).

Stream Description	SP52TA46	SP52TA47	SP52TA48	SP52TP50	SB52TA58	SB52TA59	SB52TA60
Temp (°C)	100.48	100.48	80.00	80.67	100.48	70.00	93.54
Pres (bar)	1.00	1.00	1.00	17.00	1.00	2.00	1.00
Vapor (mol/mol)	0.00	0.00	0.00	0.00	0.00	1.00	1.00
MW (g/mol)	19.07	19.07	19.07	19.09	19.07	33.68	23.28
Mole Flow (kmol/h)	5942.69	6095.13	5942.69	5951.79	152.38	16.02	270.48
Mass Flows (kg/h)							
TOTAL	113336	116243	113335.91	113642.92	2906.07	539.59	6297.75
CARBO-01	0.58	0.59	0.40	0.39	0.01	439.62	2413.26
HYDRO-01	0.00	0.00	0.00	0.00	0.00	0.22	0.01
METHA-01	0.00	0.00	0.00	0.00	0.00	56.22	2.54
WATER	103181	105828	103185.87	103257.58	2645.69	43.53	3881.94
POTAS-01	0.00	0.00	0.00	0.00	0.00	0.00	0.00
$H3O^+$	0.00	0.00	0.00	0.00	0.00	0.00	0.00
K^+	5184.36	5317.29	5184.36	5317.29	132.93	0.00	0.00
OH^-	9.33	9.57	4.49	4.81	0.24	0.00	0.00
HCO_3^-	1964.79	2015.18	1947.92	1949.11	50.38	0.00	0.00
CO_3^{2-}	2996.04	3072.86	3012.88	3113.74	76.82	0.00	0.00
Mass Fractions							
CARBO-01	0.000	0.000	0.000	0.000	0.000	0.815	0.383
HYDRO-01	0.000	0.000	0.000	0.000	0.000	0.000	0.000
METHA-01	0.000	0.000	0.000	0.000	0.000	0.104	0.000
WATER	0.910	0.910	0.910	0.909	0.910	0.081	0.616
POTAS-01	0.000	0.000	0.000	0.000	0.000	0.000	0.000
$H3O^+$	0.000	0.000	0.000	0.000	0.000	0.000	0.000
K^+	0.046	0.046	0.046	0.047	0.046	0.000	0.000
OH^-	0.000	0.000	0.000	0.000	0.000	0.000	0.000
HCO_3^-	0.017	0.017	0.017	0.017	0.017	0.000	0.000
CO_3^{2-}	0.026	0.026	0.027	0.027	0.026	0.000	0.000

Table 7: Stream report for the PSA section.

Stream Description	SP53TA44	SP53TA38	SP53TA46	SP53TP35	SP53TP41	SP53TP43	SP53TP50
Temp (°C)	25.00	25.00	25.00	25.00	25.00	25.00	25.00
Pres (bar)	1.00	1.00	1.00	17.00	17.00	17.00	17.00
Vapor (mol/mol)	1.00	1.00	1.00	1.00	1.00	1.00	1.00

MW (g/mol)	15.66	15.66	15.66	15.64	15.64	15.64	15.64
Mole Flow (kmol/h)	69.98	69.98	69.98	277.87	277.87	207.89	207.89
Mass Flows (kg/h)							
TOTAL	1095.94	1095.94	1095.94	4346.92	4346.92	3250.98	3250.98
CARBO-01	2.32	2.32	2.32	9.26	9.26	6.95	6.95
HYDRO-01	4.24	4.24	4.24	16.97	16.97	12.73	12.73
METHA-01	1077.10	1077.10	1077.10	4308.41	4308.41	3231.31	3231.31
WATER	12.28	12.28	12.28	12.28	12.28	0.00	0.00
Mass Fractions							
CARBO-01	0.002	0.002	0.002	0.002	0.002	0.002	0.002
HYDRO-01	0.004	0.004	0.004	0.004	0.004	0.004	0.004
METHA-01	0.983	0.983	0.983	0.991	0.991	0.994	0.994
WATER	0.011	0.011	0.011	0.003	0.003	0.000	0.000

Table 8: By-products report.

Stream Description	SB51TA04	SB51TA32	SB51TP02	SB52TA62	SB51TA01
Temp (°C)	75.00	100.00	80.00	92.09	79.80
Pres (bar)	1.05	1.20	17.00	1.00	1.09
Vapor (mol/mol)	0.00	1.00	0.00	1.00	0.00
MW (g/mol)	18.04	23.60	18.04	23.87	18.02
Mole Flow (kmol/h)	202.19	298.05	202.19	286.50	415.41
Mass Flows (kg/h)					
TOTAL	3646.58	7033.45	3646.58	6837.34	7483.98
CARBO-01	7.15	2941.02	7.15	2852.89	0.59
HYDRO-01	0.00	8.29	0.00	0.23	0.00
METHA-01	0.55	58.77	0.55	58.76	0.04
WATER	3638.87	4025.37	3638.87	3925.47	7483.34
Mass Fractions					
CARBO-01	0.002	0.418	0.002	0.417	0.000
HYDRO-01	0.000	0.001	0.000	0.000	0.000
METHA-01	0.000	0.008	0.000	0.009	0.000
WATER	0.998	0.572	0.998	0.574	1.000

Table 9: Steam generation section.

Stream Description	QS50TP10	QS50TP12	QS50TP14	QS50TP19	QW50TA01	QW50TP05	QW50TP07	QW50TP21
Temp (°C)	100.17	100.49	100.49	100.49	15.00	72.41	95.00	100.18
Pres (bar)	1.02	1.02	1.02	1.02	1.00	1.10	1.10	1.02
Vapor (mol/mol)	1.00	1.00	1.00	1.00	0.00	0.00	0.00	0.00
MW (g/mol)	18.03	18.03	18.03	18.03	18.02	18.02	18.02	18.02
Flows (kmol/h)	399.21	5.55	360.58	33.08	44.41	662.00	662.00	262.79
Mass Flows (kg/h)								

TOTAL	7196.39	100.00	6500.00	596.39	800.00	11930.56	11930.56	4734.17
CARBO-01	7.74	0.11	6.99	0.64	0.00	7.74	7.74	0.00
HYDRO-01	0.00	0.00	0.00	0.00	0.00	0.00	0.00	0.00
METHA-01	0.60	0.01	0.54	0.05	0.00	0.60	0.60	0.00
WATER	7188.05	99.88	6492.46	595.70	800.00	11922.21	11922.21	4734.17
Mass Fractions								
CARBO-01	0.001	0.001	0.001	0.001	0.000	0.001	0.001	0.000
HYDRO-01	0.000	0.000	0.000	0.000	0.000	0.000	0.000	0.000
METHA-01	0.000	0.000	0.000	0.000	0.000	0.000	0.000	0.000
WATER	0.999	0.999	0.999	0.999	1.000	0.999	0.999	1.000

Table 10: Fluids list for the calculation of energy balance.

ID	Streams (in-out)	ΔH (kW)	Tin (°C)	Tout (°C)	Description
1	FR51TA09	802	60	152	Feed heating through the second bed
2	-	282	152	120	Feed cooling after the second bed
3	-	865	120	217	Feed heating through the third bed
4	-	603	217	150	Feed cooling after the third bed
5	-	518	150	208	Feed heating through the fourth bed
6	-	429	208	160	Feed cooling after the fourth bed
7	-	377	160	202	Feed heating through the fifth bed
8	-	20	202	200	Feed cooling after the fifth bed
9	-	671	256	200	Products cooling after first bed
10	-	377	445	200	Second bed cooling
11	-	2918	445	190	Products cooling after second bed
12	-	518	395	190	Third bed cooling
13	-	2305	395	180	Products cooling after third bed
14	-	865	308	180	Fourth bed cooling
15	-	1270	308	180	Products cooling after fourth bed
16	-	802	180	166	Fifth bed cooling
17	SP51TA20-21	629	166	97	Products cooling after reaction
18	SP51TA21-22	4950	97	80	Water condensation (1)
19	SP51TA23	444	193	110	1st compression stage cooling
20	-	351	224	160	2nd compression stage cooling
21	-	480	283	200	3rd compression stage cooling
22	SP51TP25	638	200	160	Gas cooling after compression (1)
23	SP51T30-32	2300	160	80	Gas cooling after compression (2)
24	SP51TP25-27	92	80	71	Water condensation (2)
25	SP51TP41-40	1639	84	70	Saturated carbonate solution degasing
26	SP52TP40-44	2414	70	90	Rich-lean carbonate solution heat exchange
27	SP52TP46-48	2414	100	80	Rich-lean carbonate solution heat exchange
28	SP52TP44-45	267	81	25	Sweet gas cooling
29	QW50TP07	314	72	95	Process condensate heating (1)
30	-	210	99	100	Process condensate heating (2)
31	QW50TP21	3944	100	101	Steam generation

32	456	101	100	Steam generator dispersion (by fixing vaporized fraction)
33	3226	114	30	Liquid gas section heat sink (not included in the Pinch Analysis)